Energy Storage in a DNA Origami Beam to Increase the Rate of DNA Strand Displacement

---

HONORS THESIS

Submitted to

The Engineering Honors Committee\

119 Hitchcock Hall

College of Engineering

The Ohio State University

Columbus, Ohio 43210

by

Joshua Brockman

4/11/2014

Abstract

DNA origami, the programmed self-assembly of DNA into precisely designed structures, has the potential to create nanoscale devices with diverse functions including controlled drug delivery and molecular computing. A major current direction of DNA origami is integrating dynamics, largely accomplished through DNA strand displacement, the controlled dislodgment of DNA strands by other strands. However, DNA strand displacement is a slow process driven by random thermal fluctuations and therefore occurs on the timescale of tens of minutes or hours. The goal of this work is two-fold: 1) to design a DNA origami nanostructure that stores energy by mechanical deformation (much like a compressed spring), and 2) to use the energy stored in the structure to speed the process of DNA strand displacement. A spring-like nanostructure was designed based on a 7-helix bundle of DNA that stores mechanical energy through bending deformation much like a leaf spring. The device is bent by connecting the ends with single-stranded DNA (ssDNA). The degree of bending deformation, and hence the mechanical energy stored is controllable by the length of the ssDNA connection. The stored energy can then be used to accelerate displacement of the fluorescently-labeled DNA strand holding the beam into the bent conformation. Strand displacement reactions were allowed to run for several time points up to 40 minutes. Strand displacement was quantified via fluorescence imaging of the Alexa 555-labeled strand and the fluorescence data was analyzed to assess the speed of strand displacement. Fluorescence data indicates a twentyfold decrease in the time constant for the mechanically deformed bundle compared to an unstressed control, indicating the stored mechanical energy expedited DNA strand displacement. Ultimately, these results may provide a means to speed molecular computing and facilitate targeted drug delivery.

Acknowledgements

I would like to thank Professor Carlos Castro for his mentorship throughout my undergraduate career. He has been instrumental in guiding and assisting my undergraduate experiences and inspired me to continue pursuing a career in research. I would also like to thank the member of the Nanoengineering and Biodesign Lab for their support throughout my thesis research. I would like to extend special thanks to Chris Lucas, Mike Hudoba, and Alex Marras for teaching me all I know about working in a laboratory environment.

Finally, I would like to thank Professor Samir Ghadiali for mentoring me throughout this research project and for serving as my co-advisor.

Table of Contents

Table of Figures

1. Introduction

1.1 DNA Origami Background

DNA, one of the fundamental building blocks of biological systems, is well known for encoding the genetic instructions necessary for life. The same interactions that encode biological function and characteristics also make DNA amenable to programmed self-assembly. Early efforts in structural nanotechnology utilized artificially synthesized DNA sequences to create 2D DNA crystal arrays and mechanical nanodevices [1,2]. These early works in structural nanotechnology exploited the well-understood Watson-Crick base pairing of DNA in order to create precisely designed nanoscale structures via molecular self-assembly. However, every DNA strand in these early devices had to be individually designed and synthesized.

Recently, a more efficient design and fabrication technique called DNA origami has emerged in DNA nanotechnology. In this approach, a long (~7000-8000 bases) strand of single stranded DNA (ssDNA), called the scaffold, is folded into a desired three dimensional conformation by binding many shorter (~30-50 bases) complementary ssDNA strands, called staples [3]. The staples are designed to be piecewise complementary to the scaffold to drive folding of the scaffold into a more compact structure. This concept is illustrated in Figure 1.

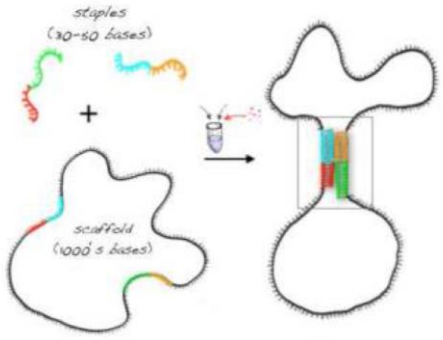

Figure 1: Using Watson-Crick base pairing for scaffolded DNA origami. [Castro 2011 presentation]

The binding of many staples to nonadjacent sections of the scaffold constrains the scaffold into a designed shape. DNA origami structures are therefore formed from many interconnected bundles of double-stranded DNA (dsDNA). The routing of the scaffold and binding of the staples in three dimensions utilized in DNA origami designs are depicted in Figure 2.

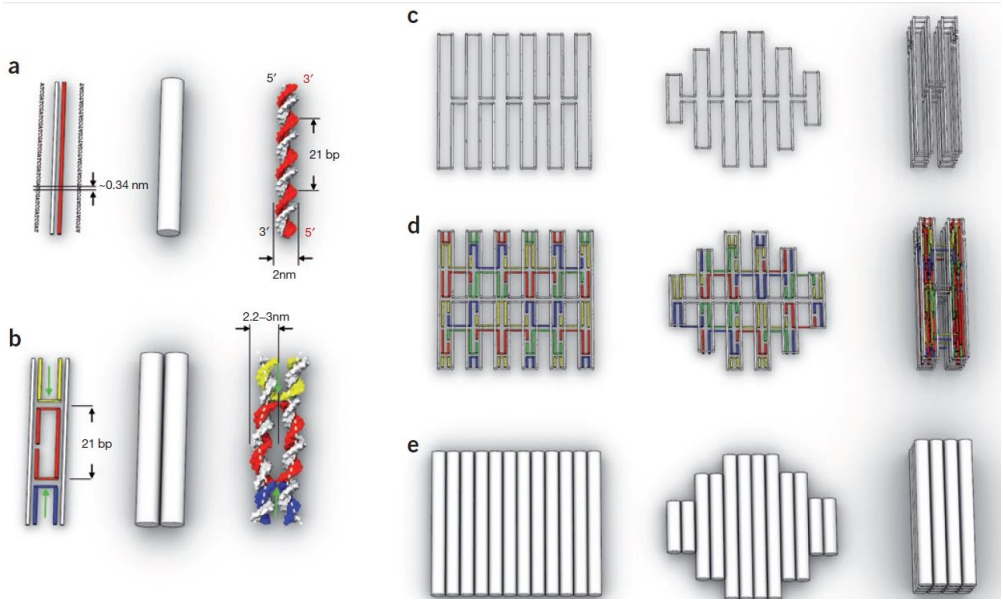

Figure 2: (a) DNA sequences are depicted as tubes. Scaffold is represented as a white tube while the staples are represented in color. (b) The staples bind to non-adjacent sections of the scaffold and crossover between scaffold rows to form 3D objects. (c) the scaffold can be routed into a variety of 2D and 3D shapes. (d) Depiction of staples bound to the routed scaffold. (e) Double-stranded scaffold-staple helices in DNA origami structures are depicted schematically here as white cylinders. [Castro 2011]

Figure 2 illustrates the general design process of scaffold-based DNA origami. Generally, the single-stranded scaffold is routed in a loop such that it takes the desired shape. Examples of routed scaffolds are depicted in Figure 2c. Staples are then added to the design. The staples cross over between adjacent helices of the scaffold and will hold the scaffold in the desired three dimensional shape. The binding of the staples to the routed scaffold is shown in Figure 2b and 2d. The resulting 3D shapes resulting from the staple-scaffold binding are shown in Figure 2e.

DNA origami has been used to build a wide variety of nanoscale 2D and 3D shapes [3,5,6]. These nanoscale objects are commonly observed through atomic force microscopy (AFM) and transmission electron microscopy (TEM). Some examples of 3D DNA origami nanostructures are shown in Figure 3 [6].

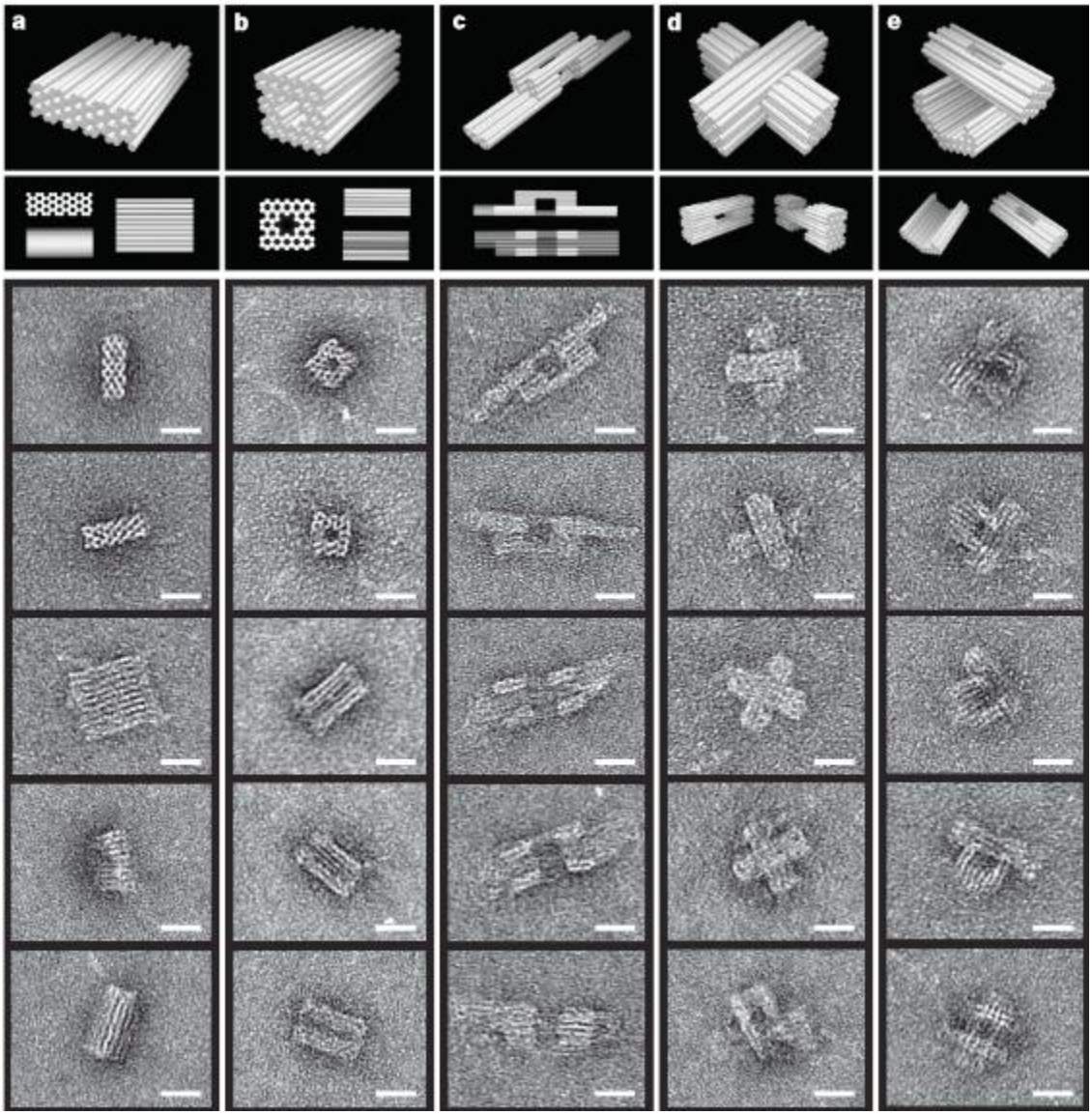

Figure 3: This figure depicts a variety of nanoscale objects created through scaffolded DNA origami. Columns (a) – (e) depict a 3D model of a shape at the top of the column. Each cylinder in the models represents a double stranded DNA helix. The rows of each column depict TEM images of the shape modeled at the top of each column. Each scale bar is 20 nm [Douglas 2009].

While the majority of DNA origami structure to date, including all of the shapes depicted in Figure 3, have focused on static structures, integrating dynamic functionality has recently garnered a great deal of interest in the field of DNA origami [7]. For example, the controllable DNA hinge under development in the Nanoengineering and Biodesign Lab integrates dynamics by connecting stiff DNA components with flexible single-stranded DNA connections that allow flexible motion in one rotational degree of freedom. This approach constrains motion; however in that degree of freedom motion is still dominated by random thermal fluctuations.

The most common approach to actuate DNA nanostructures is DNA strand displacement. DNA strand displacement is the controlled dislodgment of DNA strands by other strands with higher binding affinity [8]. The total binding energy of one strand to another is related to the composition of the DNA bases—the guanine-cytosine interaction is stronger than that of adenine and thymine—and the length of the hybridizing strands. Therefore, a strand that is bound to a portion of another strand can dynamically be displaced if a fully complementary strand is introduced in solution. This process of displacement, commonly called branch migration, is depicted in Figure 4.

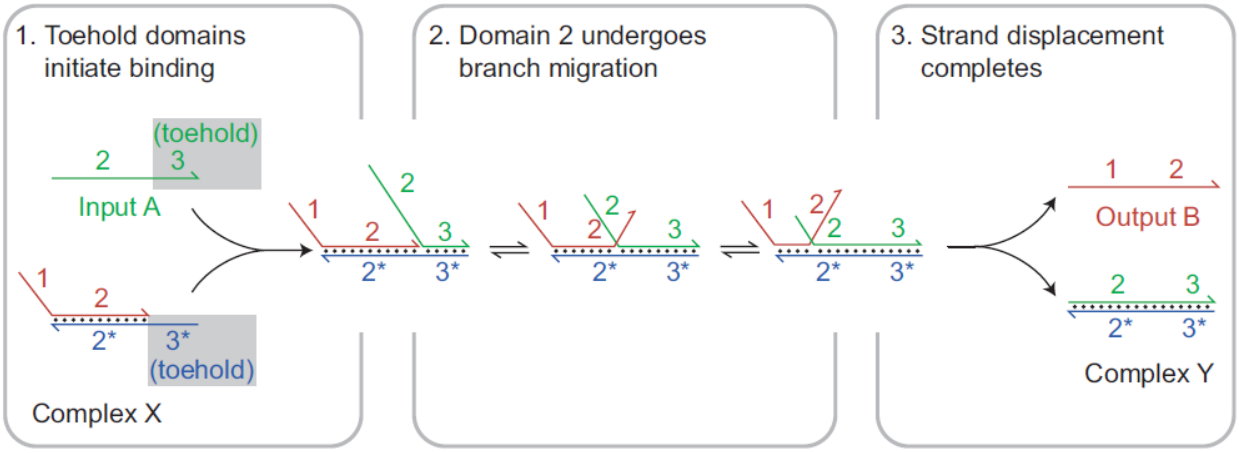

Figure 4: Branch migration in DNA strand displacement reactions. [Zhang and Seelig, 2011]

To initiate the strand displacement reaction, DNA nanotechnology frequently utilizes toeholds, single-stranded domains of staples that are exposed to solution and may bind to displacing strands. In panel 1 of Figure 4, the blue strand has a toehold that is complementary to the green displacement strand. During a strand displacement reaction, the green strand will first bind to the exposed toehold. Following the binding of the toehold, the displacement reaction will proceed via base-by-base displacement termed brand migration. During brand migration, the red and green strand will randomly bind and unbind due to random thermal fluctuations. Over time, the green strand will claim more and more of the bases formerly bound to the red strand. Strands with greater binding affinity, here green has higher affinity than red, will displace lower-affinity strands; however, during the displacement of each individual base—an adenine on one strand displacing an adenine on the other, for instance—the binding affinities of the individual bases are identical. No energetic bias for the forward displacement reaction exists for the displacement of individual bases. DNA strand displacement through branch migration is therefore a very slow process, with a timescale generally measured in tens of minutes or even hours [8]. Figure 5 illustrates the timescale of DNA strand displacement.

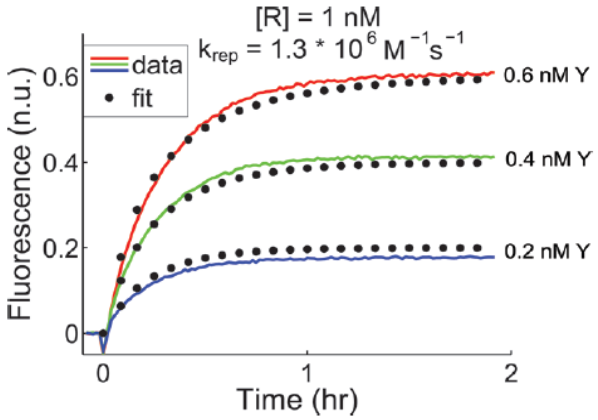

Figure 5: DNA strand displacement reactions require up to an hour to run to completion. Here, the fluorescence of a reporter that binds to strand displaced by strand Y (at the concentration indicated to the right) is measured to monitor the progress of the strand displacement reaction [Zhang and Winfree 2009].

Despite the limitations imposed by the long timescale, DNA strand displacement has recently been used in the creation of a functional DNA origami robot capable of recognizing specific proteins on target cells and then releasing molecular payloads to those cells [9]. Additionally, DNA strand displacement was used in diagnostic structures with YES and AND logic gates capable of recognizing micro-RNA's indicative of heart failure as inputs [10]. These two structures are depicted in Figure 6. For a review of more recent DNA origami research, including more functional nanostructures, see the 2013 review by Veikko Link and Hendrik Dietz [11].

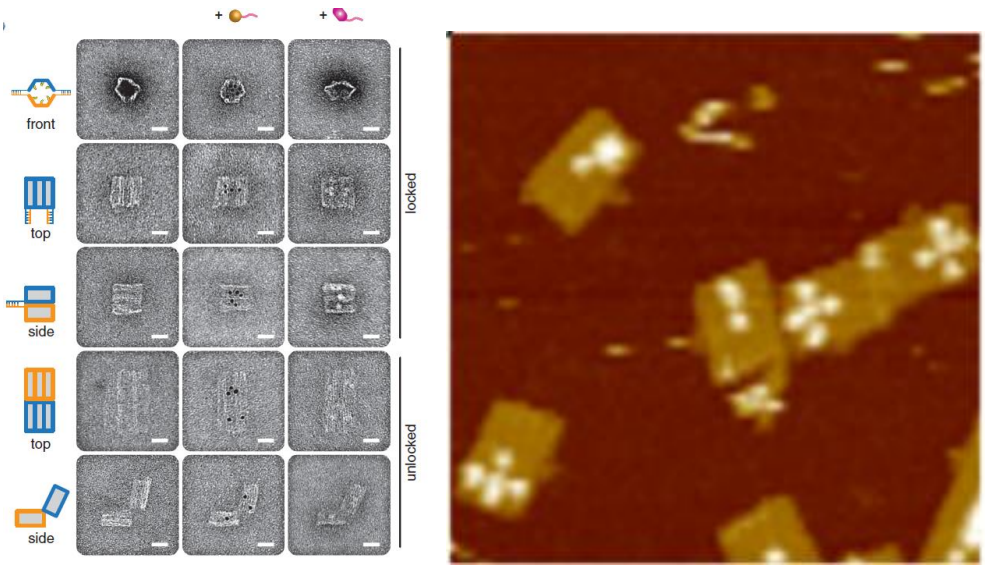

Figure 6: Functional DNA origami structures. (Left) Panel depicts molecular robot capable of carrying molecular payloads. Left column: no payload; middle column: gold nanoparticles; right column: antibody fragments. The top 3 rows show the locked structure while the bottom two rows have been unlocked by opening aptamer locks [Douglas et al 2012]. (Right) Panel depicts DNA origami microRNA detection devices utilizing an AND logic gate. The panels display the "+" sign when both diagnostic microRNA's for heart failure (miR-21 and miR-195) are present [Wang et al 2014]

1.2 Objectives and Significance

DNA strand displacement has a wide range of potential applications. As mentioned previously, DNA origami has applications in controlled drug delivery and diagnostics [9,10]. Additionally, DNA based walkers that utilize strand displacement events to take individual steps

have potential to achieve transport of nanoscale objects for applications in nanomanufacturing or biosensing have been created [12].

Furthermore, DNA strand displacement has myriad applications in molecular computing. DNA strand displacement has been used to read inputs and create outputs for molecular AND, OR, and NOT logic gates [13]. DNA logic gates could be used in biosensing, diagnostics, and for controlling drug delivery.

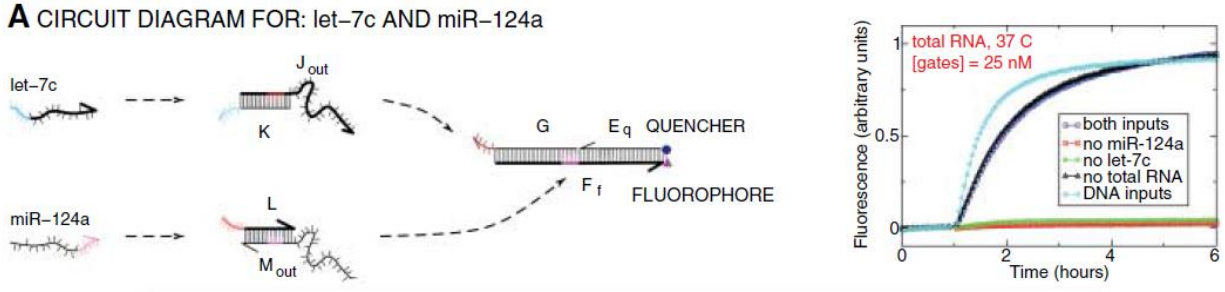

Figure 7: Molecular computing can be accomplished using DNA strand displacement.Here two microRNA's, let-7c and miR-124a, serve as the inputs to a logical AND gate created from a small caascade of DNA strand displacement reactions. The plot to the right displays the fluorescence of the fluorophore as a function of time. The gate functions at 37 degrees celsius, with RNA or DNA, and is not impeded by the presence of physiological levels of total RNA. The displacemetn cascade requires more than an hour to operate.

Figure 7 demonstrates a cascade of DNA strand displacement reactions capable of creating a logical AND gate; however, the cascade requires over an hour to operate under physiological conditions, shown by the purple curve [13]. Thus, the utility of this technique, like the utility of DNA walkers and drug delivery devices, is limited by its long timescale. As shown in Figure 5 and Figure 7 DNA strand displacement requires 10's of minutes to hours to operate. Moreover, molecular computing, one of the most exciting applications of DNA strand displacement, relies on cascades of displacement reactions, further increasing the amount of time required. This research aims to develop a method to expedite DNA strand displacement to enhance the function of nanoscale robots and computational strand displacement cascades.

The overall goal of this thesis was to develop a novel approach to accelerate the timescale of DNA strand displacement. To achieve this goal, we developed two specific aims: 1) to design

a DNA origami nanostructure that stores energy by mechanical deformation (much like a compressed spring), and 2) to use the energy stored in the structure to generate a force that can accelerate the process of DNA strand displacement. Accelerating DNA strand displacement would greatly enhance the utility of DNA origami in both research and clinical settings.

1.3 Thesis Overview

Chapter 2 of this thesis discusses the research methodologies including the design of the DNA bow, the process of manufacturing and imaging the bow via TEM, and the procedure followed during fluorescence experimentation. Chapter 3 presents the results obtained through TEM imaging and during fluorescence experimentation. Chapter 4 discusses the implications of the results and proposes future work.

Chapter 2. Device Design and Experimental Methods

This section covers the design, fabrication, and imaging of a DNA beam capable of storing mechanical energy through a tunable amount of bending deformation, hereafter called the DNA bow. The experimental procedures by which the displacement rates were experimentally measured are also covered within this section.

2.1 Design of the DNA Bow

A deformable DNA origami beam, termed the DNA bow, consisting of a bundle of 7 double-stranded DNA (dsDNA) helices was designed using caDNAno [10]. CaDNAno is a program that facilitates the design of DNA origami structures by enabling users to route the scaffold in the desired manner, specify staple binding, and automating the process of sequencing the staples based upon the specific scaffold/staple routing. A schematic of the caDNAno design of the DNA bow is shown in Figure 5. A cross-section of the bow is shown in the inset images at the bottom right of Figure 5.The bow was made from an 8064 base scaffold modified from an M13mp18 bacteriophage genome. The structure contains 210 staples. The contour length of the bow is slightly less than 350 nm. The contour length of the ssDNA “string” is about 385 nm without the addition of bending staples and is composed of 672 single-stranded bases.

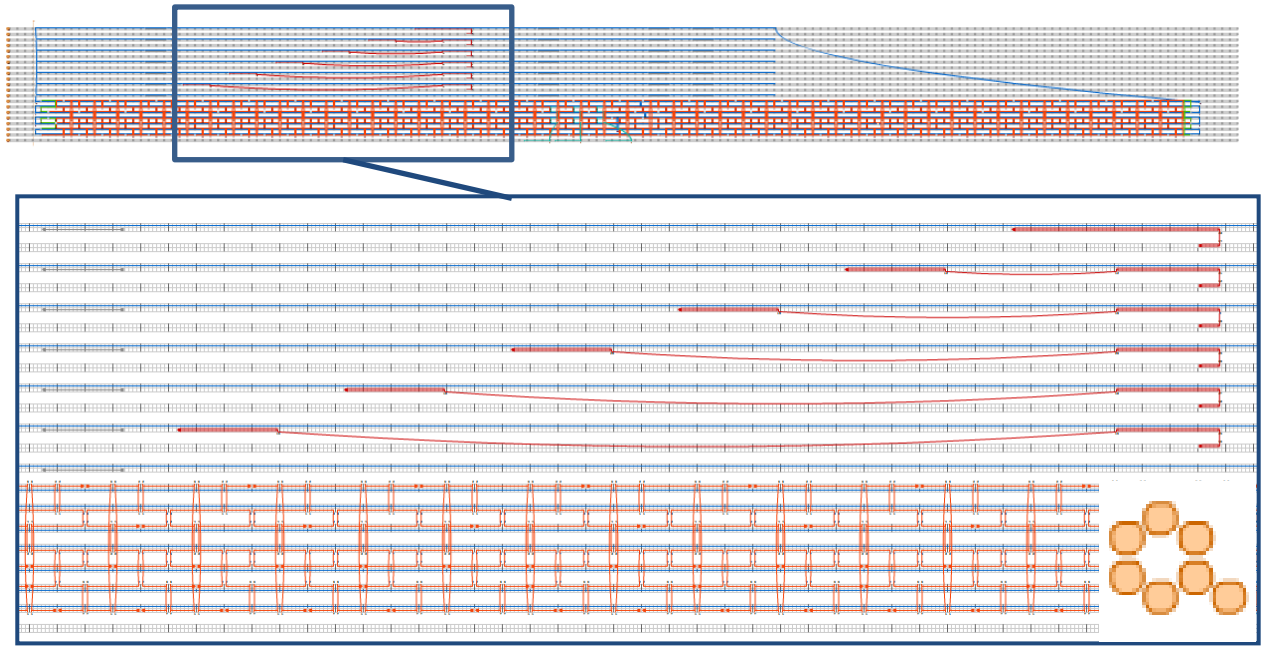

Figure 8: This figure depicts the caDNAno design of the DNA bow. The expanded view shows a close up of the staples that allow the end-to-end length of the bow to be adjusted. These staples, termed bending staples, are shown in red and bind to a single stranded region of the scaffold in order to draw the ends of the beam together. Each experiment only contained one of these bending staples. Inset: cross-section of the bow, the string is located opposite to the protruding helix.

The ends of the beam were connected by a length of single-stranded scaffold, termed the "string." A set of bending staples were designed to change the length of the single-stranded scaffold connection between the ends of the bow. These bending staples, depicted in red in Figure 5, shorten the end-to-end length of the bow by introducing loops into the ssDNA string. The bending staple was fluorescently labeled with the fluorophore Alexa 555 to enable measurement of the removal of the bending staple by DNA strand displacement. A schematic of the design depicting the function of the bending staple is shown in Figure 6.

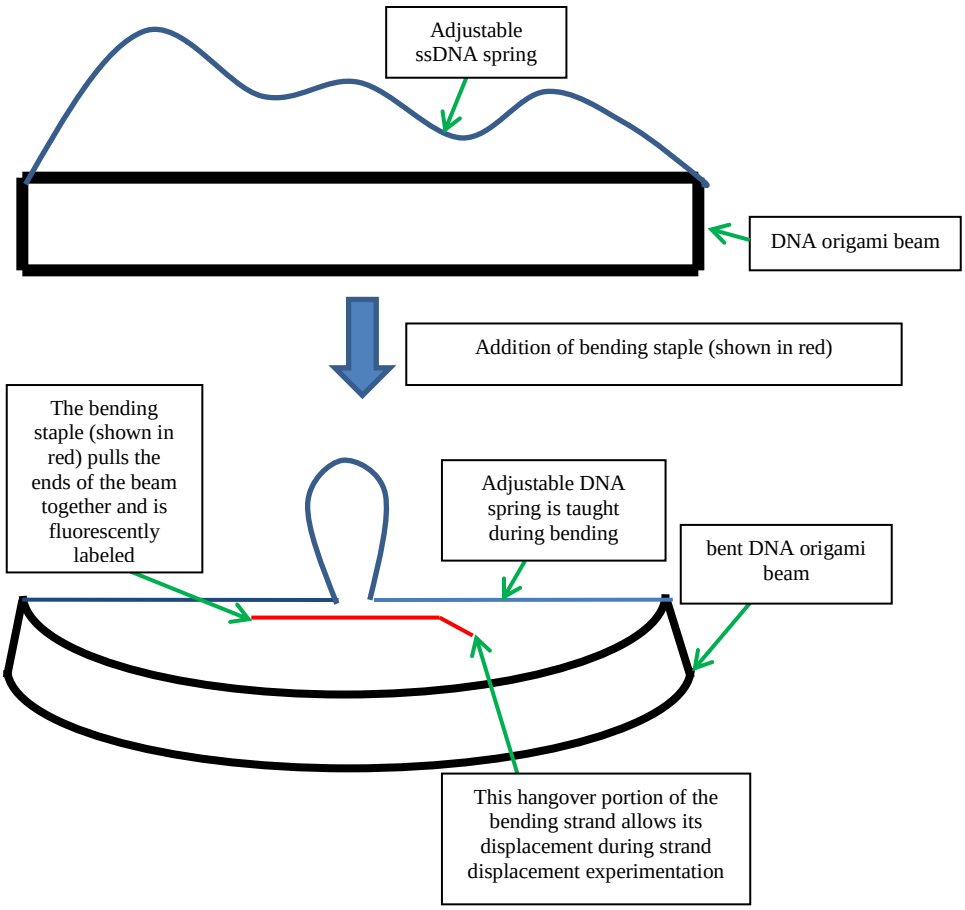

Figure 9: This schematic of the DNA bow demonstrates the function of the bending staple, shown in red. Briefly, the ends of the DNA bow are connected by a length of single-stranded scaffold. The bending staple binds to this scaffold length and tunes its end to end length by introducing loops. The tuning of the single stranded scaffold length draws the ends of the bow together, thereby storing energy in the beam.

The tunable ssDNA string functions as an entropic spring—similar to previously reported tensegrity structures [16]—that sustains a force to deform the bow and consequently store mechanical energy. The length of the ssDNA string can be decreased by incorporating the bending staples. Decreasing the length of the ssDNA string generates a force to draw the ends of the bow together, thereby bending the bow. In the bent conformation, this bow stores energy due to mechanical bending deformation, much like a bow and arrow, and the process of binding bending staples to the tunable DNA strand is analogous to pulling the string of a bow, a process depicted graphically in Figure 9. The bending cases and deformations imposed on the bow are described in table 1.

Table 1: Bending conditions and imposed deformations for the DNA bow

test condition	dsDNA added	ssDNA skipped in loop	length (nm)	deformation (nm)
double stranded structure	-------	-------	348.362	-------
single stranded "rope"	-------	-------	386.856	-------
1	53	0	372.758	14.098
2	53	42	347.558	39.298
3	53	84	322.358	64.498
4	53	126	297.158	89.698
5	53	168	271.958	114.898
6	53	210	246.758	140.098

2.2 Creating the Bow

The sequences of the 210 staples were generated using caDNAno. The staples were synthesized by MWG eurofins. An 8064 base modified M13mp18 bacteriophage genome was used as the ssDNA scaffold for the bow while a 7249 base M13mp18 bacteriophage genome scaffold was used to create an unstressed control structure. The unstressed control was a 7249 dsDNA loop that incorporated the same fluorescently labeled bending staple as the DNA bow. The DNA origami structures were folded by adding the scaffold at 20 nM concentration and staples at 10-fold excess relative to the scaffold (each staple was at a final concentration of 200 nM in the reaction) to a folding reaction containing 5mM NaCl, 5mM TRIS, 1mM EDTA, and 18 mM $MgCl_2$ dissolved in double-distilled water. The reaction solution was heated to 60^{o} C and the temperature was decreased to 4^{o} C over the course of 4.5 days in a thermal annealing ramp. This procedure was adapted from protocols developed by [3].

In order to create nanostructures with stored mechanical energy, the bow was folded in the high-energy bent conformation during the folding ramp. During the thermal annealing ramp,

ssDNA staples attach to the ssDNA scaffold in an order dependent on their melting temperature. The melting temperature of a staple is directly related to its length—a fact that was exploited in the creation of the DNA bow. The bending staple (the staple that holds the bow in the bent conformation, shown in red in Figure 9) was designed to be one of the longest staples in the structure, with 53 bases bound to the scaffold. As the temperature slowly decreased during the thermal ramp, the bending staple would therefore be one of the first staples bound to the scaffold; as the temperature decreased further, the other staples should then bind to the scaffold after the binding of the bending staples to create a bent bow at the end of the thermal annealing ramp.

2.3 Purifying the Structures

Following the thermal ramp, folded structures were purified in a 2% agarose gel via gel electrophoresis. A 70 V potential is applied across the gel during electrophoresis, drawing the negatively charged DNA towards the positive electrode. Figure 10 depicts an image of gel electrophoresis, cooled in an ice bath to prevent the gel from melting. In Figure 10 the negative electrode was located on the left and the positive electrode was located on the right.

Agarose gel electrophoresis separates DNA by size by drawing the negatively charged DNA through the porous agarose gel. An image of an agarose gel that was used to purify the DNA bow is also shown in Figure 10 (right). During electrophoresis, excess staples, which are very small relative to the DNA origami structure, move quickly through the agarose gel and are located in the large, bright bands near the right side of the gel (red box). In comparison, the larger DNA bow travels slower than the free DNA and is located in the tight bands indicated by the yellow box.

DNA origami nanostructures were purified using freeze and squeeze centrifucation tubes (BioRAD). In summary, the structure bands were cut out of the agarose gel using a scalpel, crushed using a plastic pestle, and then added to the purification tubes and centrifuged at 12,000 G's for 5 minutes through a filter with a pore size large to allow DNA origami structures to pass through, but small enough to prevent agarose from running through.

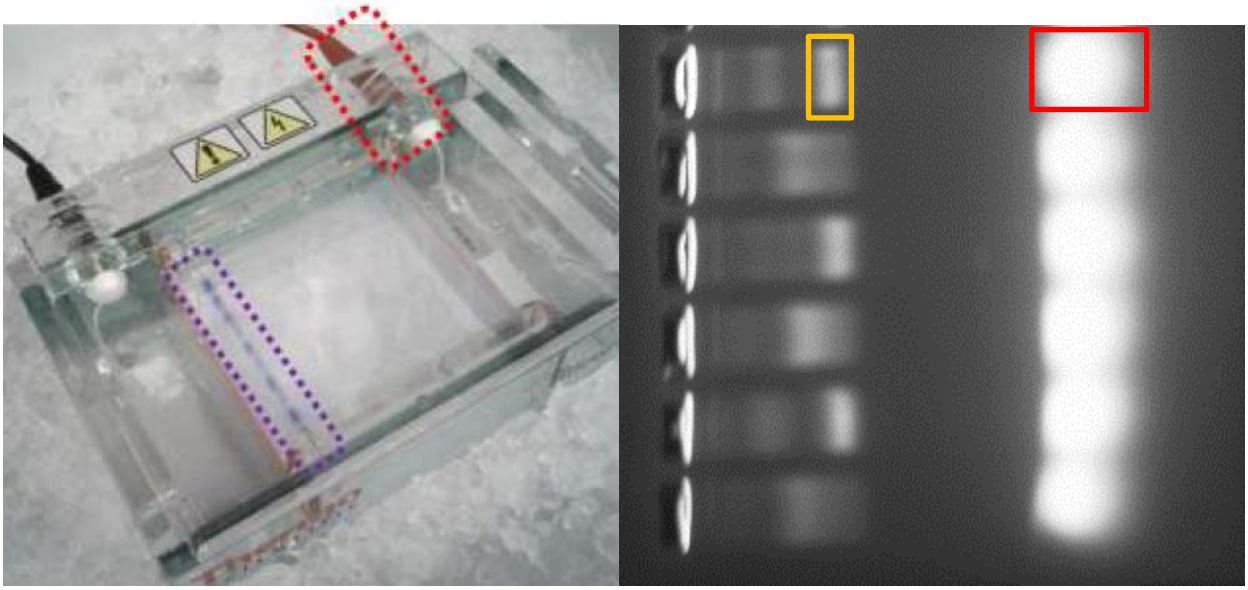

Figure 10: Gel electrophoresis was used to purify the DNA origami structures. On the right, an image of the gel electrophoresis rig is shown [Turowski 2012]. The negativeelectrode is located on the left while the positive electrode is on the right. On the right of this figure, an ethidium bromide stained agarose gel that was used to purify the DNA bow is shown. The red box surrounds a band of free DNA while the orange box surrounds the structure bands that were cut out of the gel in order to purify the structures.

Structures for fluorescence imaging were purified via polyethylene glycol (PEG) purification. Briefly, following the folding ramp, 50 µL of 15% PEG was added to 50 µL of structures. The resulting mixture was centrifuged at 16,000 G's for 30 min. Following centrifugation, the supernatant was removed and the structures were resuspended in 1xFOB + 18 mM $MgCl_2$. The DNA bow was PEG purified twice in succession while the unstressed control structures were PEG purified once.

2.4 Imaging the Structures

To verify that the structures were folded correctly, the purified DNA bows were imaged via a transmission electron microscope (TEM) at Ohio State's Campus Microscopy and Imaging Facility (CMIF). Prior to imaging, structures were immobilized on TEM grids and negatively stained with uranyl formate. Briefly, 2 μL of agarose gel purified structures were placed on a TEM grid for 4 minutes. The remaining moisture was removed with filter paper and the grid was washed with 10 μL of 2% UFo and then stained with 20 μL of 2% UFo for 30 seconds. The structures were then imaged at 49000x - 68,000x magnification.

2.5 Fluorescence Experimentation

The time dependency of DNA strand displacement on the stored mechanical energy was examined via bulk fluorescence imaging using a Typhoon gel fluorescence imager (General Electric). The fluorophore Alexa 555 was attached to the bending staple holding the bow in the bent conformation. The extent of displacement was determined by measuring the intensity of Alexa 555 fluorescence co-located with the structure band following displacement reactions that had been allowed to run for varying amounts of time.

During a displacement reaction, a 10x excess (relative to the DNA bow concentration) of the reverse complement of the bending staple, referred to as the displacement strand, was added to a solution containing the DNA bow. The displacement reaction mixture was then allowed to sit at room temperature for a specified amount of time. Displacement reactions were run for 30 seconds and 2, 5, 20, and 40 minutes, during which time bending staples were displaced from the single stranded scaffold connecting the two ends of the bow.

During each fluorescence experiment, the 40, 20, and 5 minute reactions were started by the addition of the displacement staples and were all halted at the same time by the addition of gel loading dye to each reaction, beginning with the 5 minute reaction. A portion of the reaction mixture + dye solution was then pipetted into a 2% agarose gel. The 2 minute reactions were then started. 90 seconds into the 2 minute reactions, the 30 second reactions were started. At the end of the 30 second reaction, all displacement reactions were halted by the addition of gel loading dye starting with the 30 second reaction. A portion of the 2 minute and 30 second reaction mixtures + dye solutions were pipetted into the 2% agarose gel. Structures were run through the gel by applying 70 V across the gel for 3-4 hours.

During gel electrophoresis, DNA structures separate according to their overall size. The relatively small staple strands travel the fastest through the porous gel. The excess staples are boxed in green in Figure 11. The folded DNA bow, which is relatively compact compared to misfolded structures forms the second fastest running component. The DNA bow bands are boxed in red in Figure 11. Misfolded structures and aggregates run slower showing up as a smear behind the structure band or get stuck in the well. These misfolded structure bands are boxed in blue in Figure 11. The unstressed control structure is just a double stranded loop of DNA and thus runs very slowly through the agarose gel. The control structure bands are boxed in purple in Figure 11. Staples that were not displaced during each reaction were still attached to the structure and contributed to the fluorescence of the structure band while displaced structures increased the fluorescence of the free DNA band.

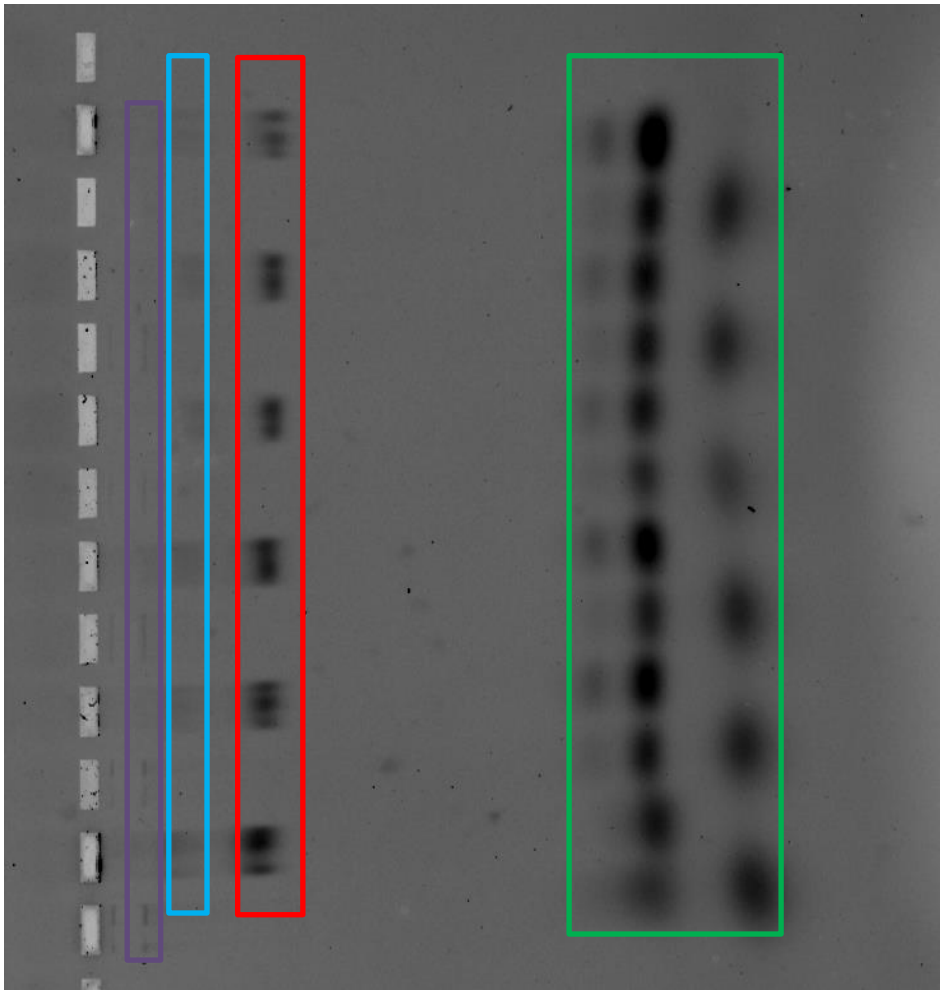

Figure 11: Gel electrophoresis separate the structures by size as they pass through the porous agarose gel. Unstressed control structures are boxed in purple. Misfolded structures and aggregates of the DNA bow are boxed in blue. DNA bow bands are boxed in red. Excess staples are boxed in green.

The extent of displacement was determined by measuring the decrease in fluorescent intensity within the structure band relative to a case where no displacement strand was added. The location and intensity of the Alexa 555 fluorescence were measured via a GE Typhoon scanner at the Ohio State Comprehensive Cancer Center. The Typhoon excited the Alexa 555 fluorophore with a 532 nm laser while the emission of the fluorophore was measured using a 545-565 nm filter.

Following fluorescence imaging on the Typhoon scanner, agarose gels were stained in order to control for the amount of DNA present in each fluorescence experiment. Agarose gels

were stained with SYBR gold. Prior to staining, a 1x solution of SYBR gold in TBE buffer was prepared. Gels were shielded from light and stained for 1 hour in the SYBR gold staining solution. Following staining, the gel was photographed using a 488 nm illumination table and a Fotodyne Express gel imaging system. To normalize for potential concentration differences in DNA structures between lanes in the gel, the concentration of DNA bows present in each fluorescence experiment was measured from the total SYBR gold fluorescence in the structure band.

Following fluorescence imaging on the Typhoon scanner, Alexa 555 fluorescence was analyzed using ImageJ. The Alexa 555 Images from the Typhoon were loaded into ImageJ and a region of interest (ROI) was created by surrounding a structure band with a rectangle. The average fluorescence within the structure band in the ROI was measured using ImageJ. The average fluorescence of the lane was then subtracted from that of the structure band to isolate the fluorescence due to the Alexa 555 bound to the DNA bow. The image analysis process is illustrated in Figure 12.

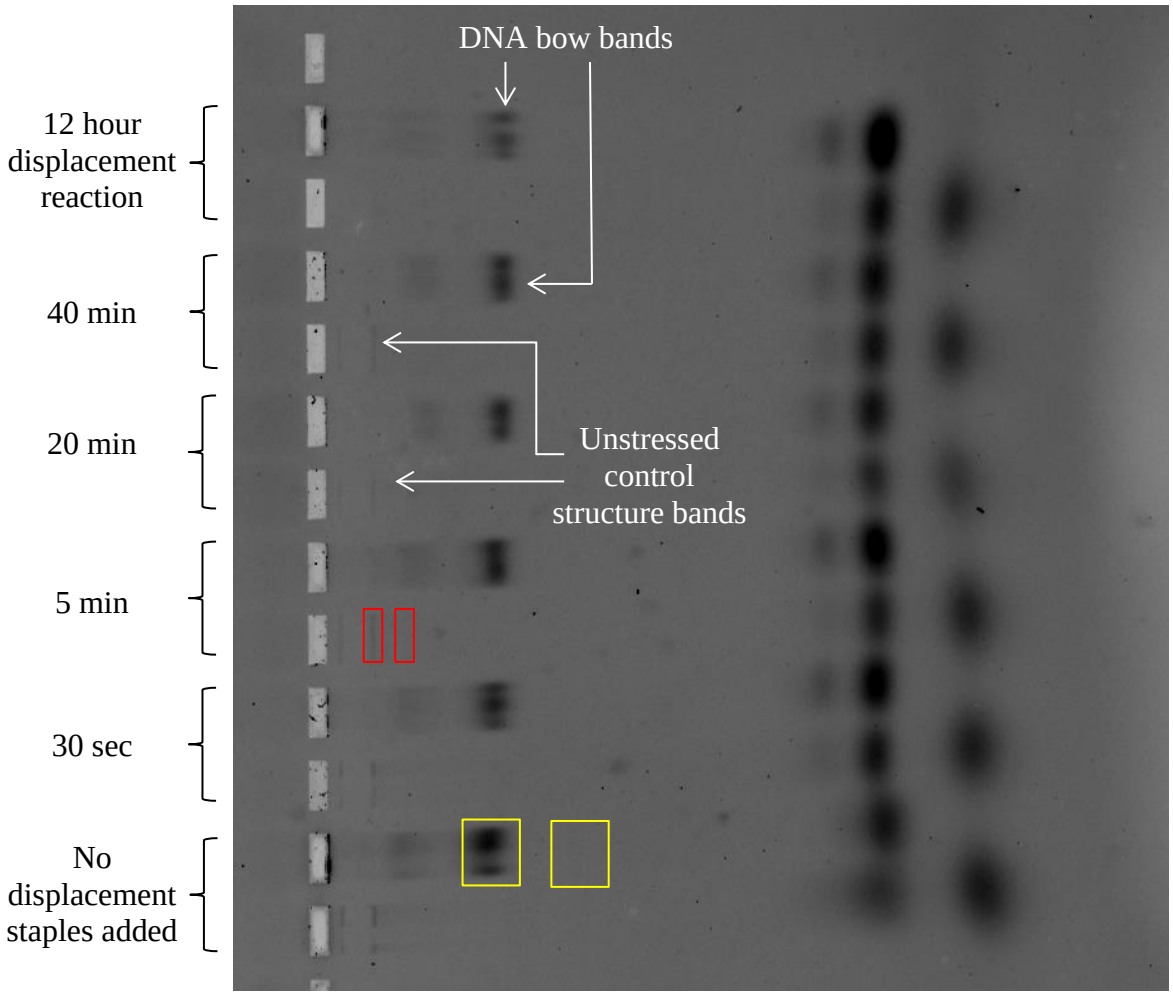

Figure 12: This figure depicts image analysis of Alexa 555 fluorescence. The red boxes were used to find the average fluorescence of the unstressed control structure and to subtract the background fluorescence. The same procedure was repeated for the yellow boxes which surround one time point of the DNA bow.

In order to control for the amount of total DNA origami structure present in each fluorescence experiment, SYBR gold staining was used to measure the total amount of DNA present in each experiment as illustrated in figure 13. The procedure of creating a ROI on a SYBR gold stain picture within ImageJ, measuring the average fluorescence within the ROI, and subtracting the background fluorescence was repeated for the SYBR gold analysis.

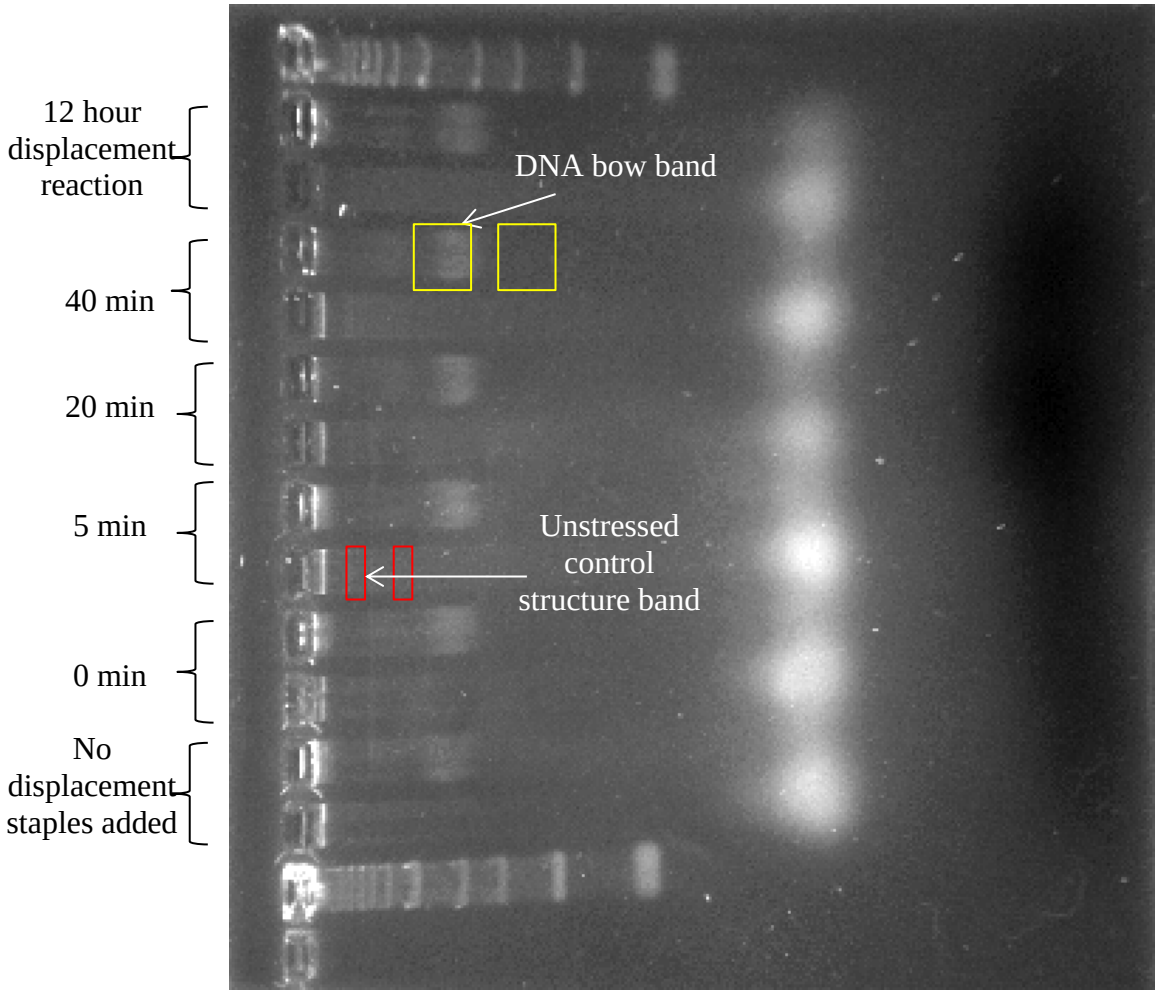

Figure 13: This figure depicts the analysis of the SYBR gold staining of the same gel shown in Figure 8. The SYBR gold staining was used as a loading control to control for the amount of structure present in each fluorescence experiment. Once again, the average fluorescence within the yellow and red ROI's was measured and the fluorescence of the background of each lane was subtracted to isolate the amount of DNA present.

Chapter 3. Results and Discussion

This chapter will outline the experimental results and discuss their implications as related to the goal of this research—to create DNA origami structures capable of accelerating DNA strand displacement.

3.1 Transmission Electron Microscopy Images

Figure 10, shown below, depicts a TEM image of the folded DNA bow at its greatest end-to-end length. In this image, no bending staples were present in the reaction solution. These bows were folded over the course of a 4.5 day thermal annealing ramp in 18 mM $MgCl_2$.

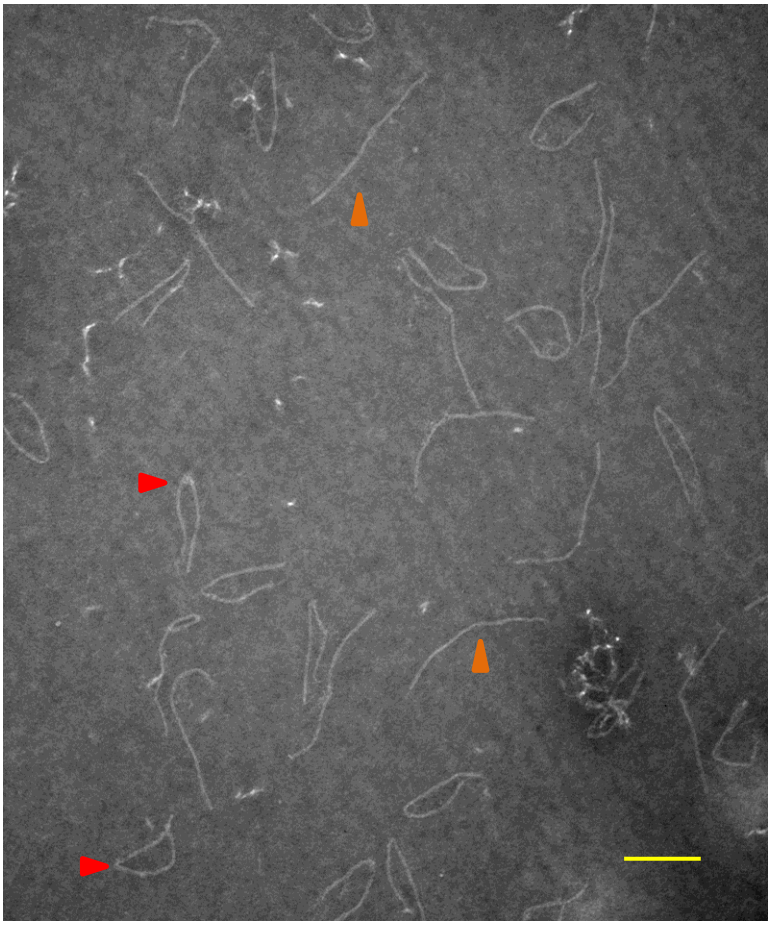

Figure 14: Folded DNA bows at 68000x magnification. The scale bar is 200 nm. This TEM image reveals one of the difficulties with the DNA bow structure. Kinking of the structure is visible in many of the TEM images. Orange triangles point to well-formed bows while red triangles point to kinked structures.

Figure 14 shows TEM images of both well-formed (orange triangles) and kinked bows (red triangles). Although it is not visible in the TEM images, the ends of the bow are connected by a length of single stranded scaffold 672 bases in length. It is possible that secondary structure—sections where the single-stranded DNA scaffold basepairs with itself to form hairpin or loops structures—may be responsible for shortening the end-to-end length of the bow in the kinked structures.

As discussed in section 2.2, staples bind in the order of their melting points during the thermal ramp. In a folding reaction, staples are present in a 10x excess relative to the scaffold. It is very possible that different segments of several identical staples bind to the scaffold in a location that only one staple should occupy. However, during the thermal ramp, the binding of staples to the scaffold decreases the energy of the system; it is energetically beneficial for only one staple to be bound to the scaffold in its designed location instead of two staples each taking half of their designed binding location on the scaffold. Even if two staples bind to one section of the scaffold, one will usually be displaced by branch migration during the thermal ramp. This process is illustrated in Figure 15.

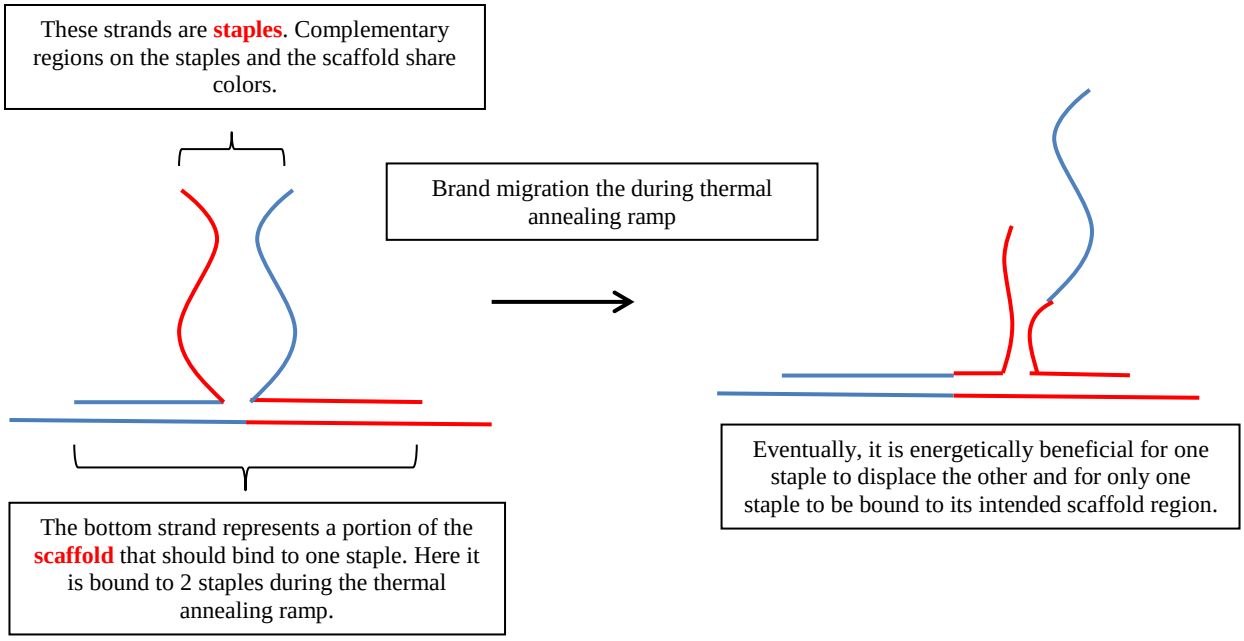

Figure 15: This figure illustrates the process by which staples bind to the scaffold during the thermal annealing ramp. The staples undergo branch migration

Typical DNA origami structures contain one scaffold and between 150-200 staples. During a folding reaction, the system attains its minimum energy by fully binding a single copy of each of those staples to the scaffold; however, the DNA bow is formed in the high-energy bent conformation during the thermal ramp. Thus during the formation of the bow there is a competition between maximizing base-pairing and minimizing mechanical energy. Each staple that binds to the scaffold decreases the free energy of the system but also increases the bending deformation of the beam, thereby increasing the mechanical energy stored within the bow. The mechanical energy is the highest at the midpoint which is subjected to the maximum applied moment due to the single-stranded scaffold connection at both ends of the bow. The kinked structures shown Figure 14 likely result from one or more locations where two copies of identical staples bind partially to the scaffold where one would suffice—as depicted in Figure 15 (left). Since in the bow system, fully binding one staple may result in a higher bending energy

than partially binding two staples, the bow may attain a local energy minimum by retaining multiple staples leading to the kinking behavior.

Other experimental conditions with increasing amounts of shortening of the tunable DNA strand were conducted. These bending conditions are shown in Figures 16–18.

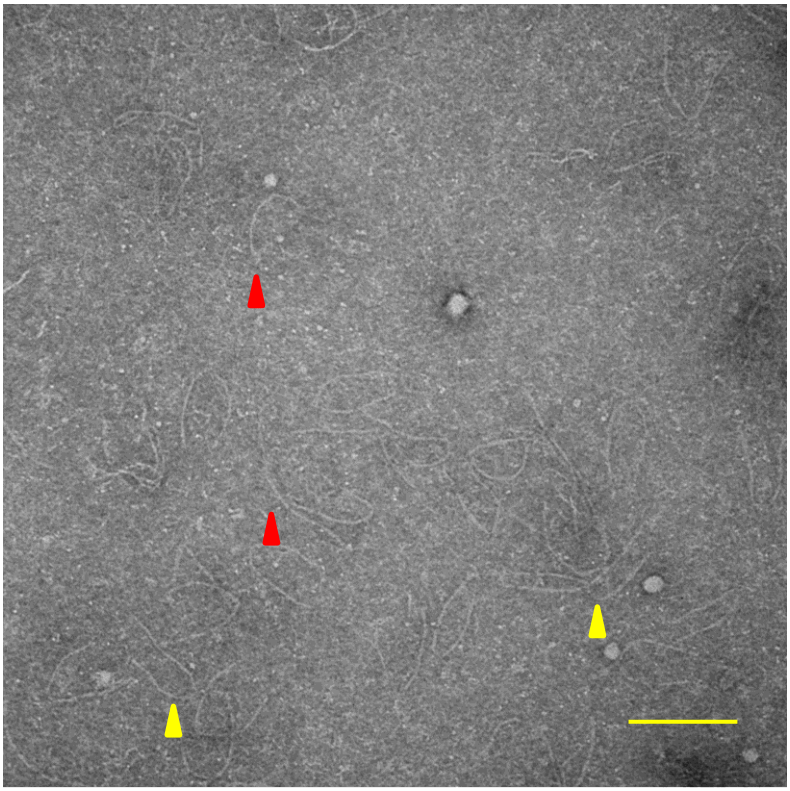

Figure 16: This figure depicts the DNA bow at 68000x magnification in a state where the end-to-end length of the tunable length of ssDNA has been decreased by about 18 nm. The scale bar is 200 nm. Red triangles point to well-formed bows, yellow triangles point to kinked bows.

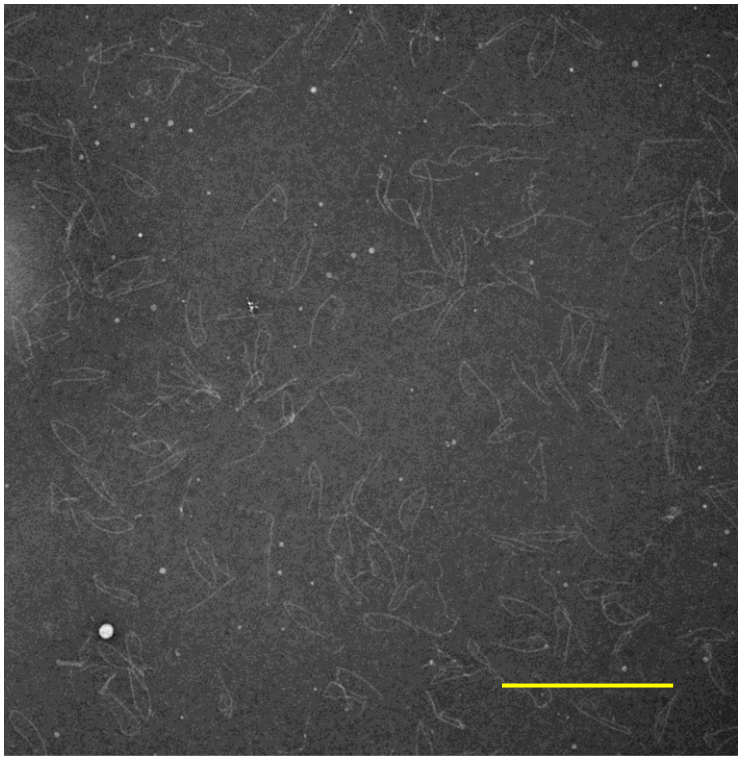

Figure 17: DNA bows are shown at 49000x magnification in a bending condition where the tunable ssDNA strand has been shortened by about 75 nm. The scale bar is 500 nm.

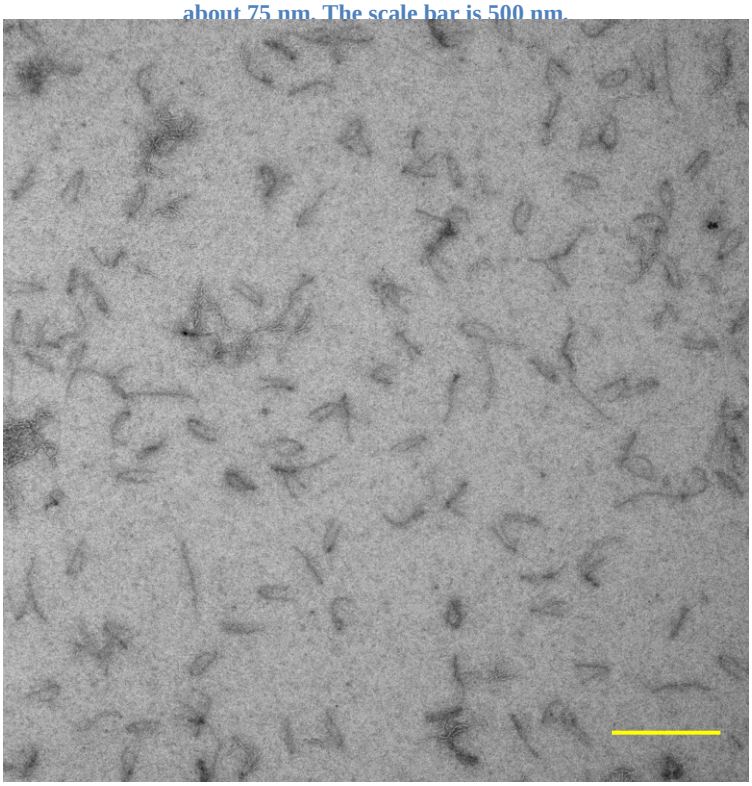

Figure 18: DNA bows are shown at 30000x magnification in a bending condition where the tunable ssDNA strand has been shortened by 115 nm. The scale bar is 500 nm.

Figure 16 shows the DNA bow in its least stressed state with the bending staple attached. In Figure 16 the end to end length of the bow has been shortened by about 18 nm. Many of the bows exhibit the gentle curve (red triangles) that was expected due to the imposed deformation; however, some of the bows in Figure 16 still exhibit kinking (yellow triangles). As the imposed deformation is increased to 75 nm in the bows in Figure 17 and 115 nm in the bows in Figure 18, the vast majority of bows appear kinked. This observation parallels the hypothesis that some bows attain an energy minimum by allowing two staples to bind to the scaffold where one would suffice in order to avoid increasing the mechanical energy stored within the beam during the self-assembly process.

Due to the prevalence of kinking in the more deformed bows, fluorescence experimentation focused exclusively on the 18 nm-imposed deformation bow. The 18-nm imposed deformation case exhibited more homogeneous folding and thus allowed more accurate measurement of the force/energy dependence of toehold-mediated strand displacement within one structure type.

3.2 Fluorescence Experiments

Following displacement reaction experimentation, the data were analyzed following the method outlined in section 2.7. The data was fit to a curve of the form of Equation 1 via a MATLAB script, included in Appendix A.

(1) $$fluorescence = A_f + (A_0 - A_f)e^{-\frac{t}{\tau}}$$

In equation 1, A_o is the initial normalized fluorescence value. A_o is equal to 1 because the normalized fluorescence at time 0, before the displacement reaction began, was the normalization factor for all other values. A_f is the final normalized fluorescence value, here taken as the fluorescence at the 40 minute time point. The parameter t is the time in seconds, and τ is

the time constant for the displacement reaction with units of seconds. The fitted time constants for the DNA bow and the unstressed control structure are shown on the next page in Table 2.

Table 2: Curve fitting parameters for fluorescence data

	Time constant, τ (sec)
DNA bow	14.12
Unstressed control	267.21

The fitted curves and raw data for the DNA bow and unstressed control are plotted in Figure 15 and 16, respectively.

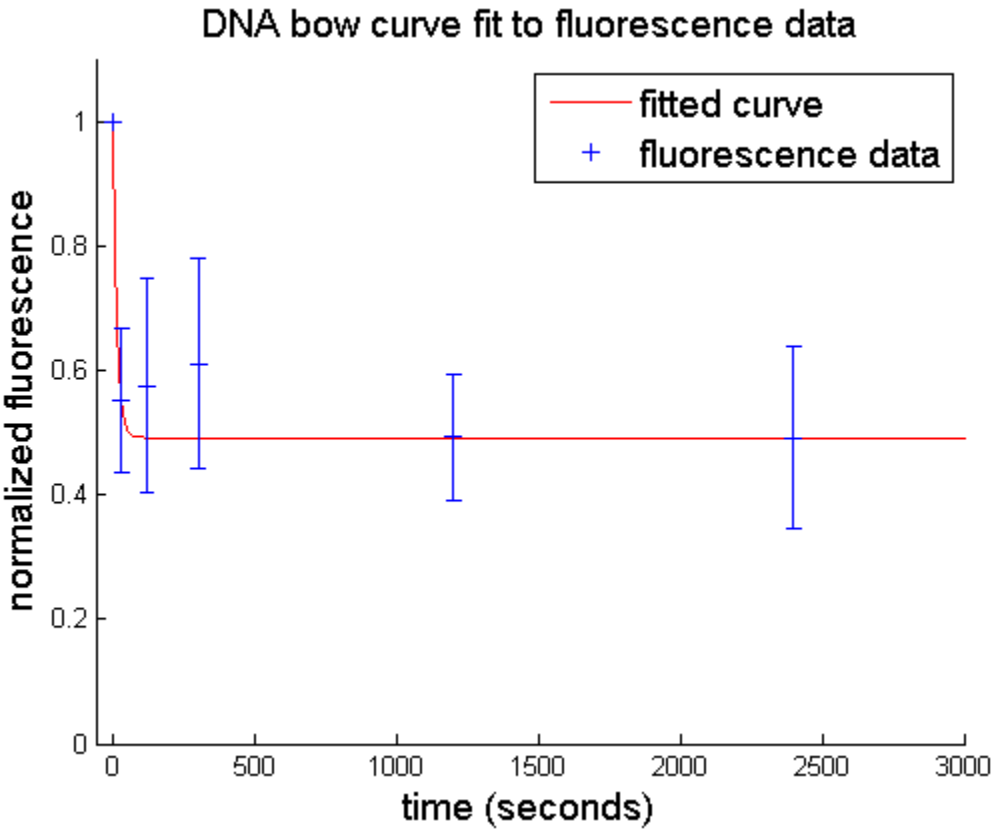

Figure 19: Fitted curve to the DNA bow fluorescence data.

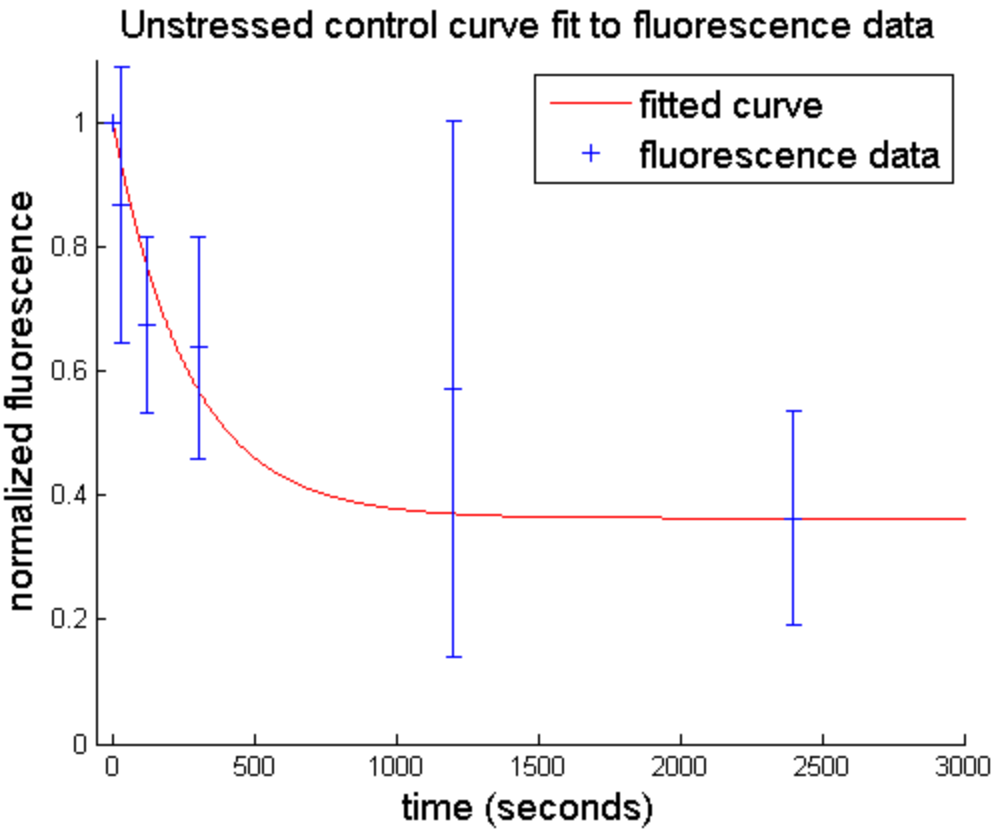

Figure 20: Fitted curve to the unstressed control structure fluorescence data.

These results show that the time constant for the high-energy DNA bow is 1/20th that of the unstressed control suggesting that the DNA bow displacement reaction progresses much faster than that of the unstressed control. This result is in agreement with the hypothesis that the energy stored within the structure would expedite DNA strand displacement. A comparison between the two fitted curves illustrating the rapidity of the DNA bow strand displacement reaction is shown in Figure 21.

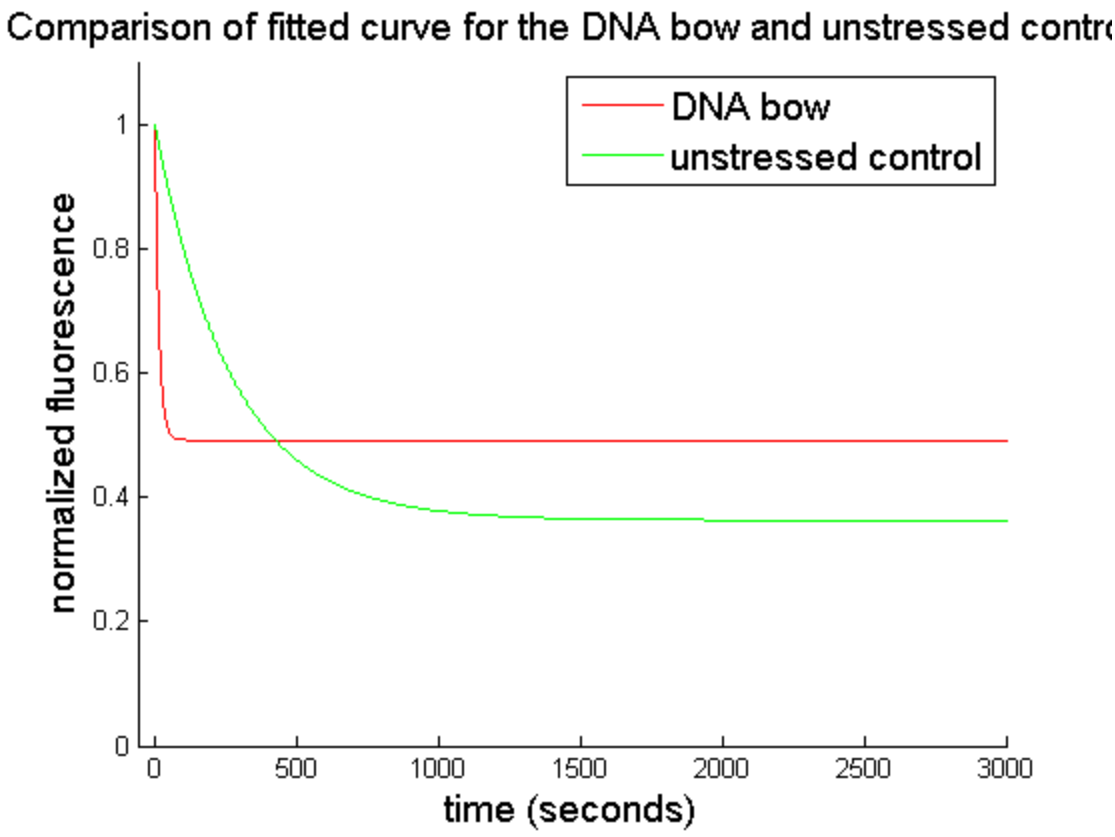

Figure 21: Comparison of the fitted curves for the DNA bow and control structure,. The displacement reaction for the DNA bow, plotted in red, was faster than that of the unstressed control.

Qualitatively, the fitted curves and fluorescence data corroborate the trend suggested by the time constants. Although the data for the unstressed control structure is very noisy, we believe the noise resulted from difficulties determining the total amount of structure present with the SYBR gold staining and is not indicative of inconsistency in the measurements. A comparison of the two fluorescence curves reveals the rapidity of the DNA bow's DNA strand displacement reaction. The normalized fluorescence for the DNA bow reaches nearly its minimum value very rapidly, perhaps even within the first minute; in contrast, the fluorescence of the unstressed control decreases more gradually and appears to reach a steady state at about 20 minutes, a timescale consistent with the literature surrounding toehold-mediated DNA strand displacement [8].

4. Conclusions

The results of fluorescence experimentation with the DNA bow suggest that the mechanical energy stored within the bow significantly increased the rate of toehold-mediated DNA strand displacement. The calculated time constant of the exponential curve fit to the DNA bow fluorescence was 14.12 seconds compared to the time constant of 267.21 seconds that was calculated for the unstressed control structure. The rate of toehold-mediated strand displacement depends on the sequence of the DNA strands and the temperature at which the reaction occurs. Here we performed all displacement reactions at room temperature; future work will more specifically explore the potential coupled effects of temperature and force. Moreover, the sequences displaced in the DNA bow and the control structure were identical for every experiment. The difference in the rate of strand displacement is therefore likely due to the force exerted on the string of the bow due to the deformation imposed on the bow. Collectively, these experiments suggest that the mechanical energy stored within the deformed DNA beam served to expedite DNA strand displacement of the Alexa 555-labled DNA strand. These experiments have therefore demonstrated the force/energy dependence of toehold-mediated DNA strand displacement reactions.

4.1 Future Work

Although these experiments illustrated the force/energy dependence of the rate of toehold-mediated strand displacement, the experimental design did not allow for accurate quantification of the actual rate of the displacement reactions. The DNA bow's measured fluorescence appears to attain nearly its minimum value at the 30 second time point. This rapid decrease in fluorescence contributed to the very low time constant for the DNA bow's displacement reaction; however, the fitted time constant suggests that the displacement reaction

had progressed significantly before even the 30 measurement period. In order to accurately quantify the rate of the DNA bow's strand displacement reaction, a technique with greater temporal resolution is required.

In order to confirm the results of the fluorescence experiments from this work, a fluorimeter could be used to measure the fluorescence as a function of time. Specifically, a fluorescence quencher could be attached to a staple on the DNA bow's "string" (the tunable ssDNA strand) while a fluorophore could be affixed to the bending staple. As long as the bending staple was attached to the string, its fluorophore's fluorescence would be quenched. Once the bending staple is displaced, however, its fluorescence would become visible to the fluorimeter. This technique could allow real-time measurement of the fluorescence resulting from the displacement of the bending staple and therefore would yield a more accurate measurement of the rate of the toehold-mediated strand displacement reaction.

Additionally, the TEM images of the DNA bow reveal that a significant portion of the bows are kinked in the middle. This kinking is likely due to the energy stored within the beam allowing the structures to find an energy minimum by failing to fold completely. In order to reduce the stress within the beam, bows with larger aspect ratios could be created to decrease the likelihood of kinking during the folding process.

These modifications—real time measurement of fluorescence with a fluorimeter combined with a higher aspect ratio bow that is less subject to kinking—could allow accurate quantification of the force/energy dependence of toehold mediated strand displacement.

References

1. Winfree, E. et al. Design and self-assembly of two-dimensional DNA crystals. *Nature* **394**, 539-544 (1998).
2. Yan, H. et al. A robust DNA mechanical device controlled by hybridization topology. *Nature* **415,** 62-65 (2002).
3. Castro, C.E. et al. A primer to scaffolded DNA origami. *Nature Methods* **228**, 221-229 (2011).
4. Castro, Carlos E. Programming Biological Self-Assembly for the Design of Nanoscale Engineering Tools. Presented at the Institute of Materials Research Biomaterials Symposium, Columbus, OH (2011).
5. Rothemund, P.W.K. Folding DNA to create nanoscale shapes and patterns. *Nature* **440**, 297-302 (2006).
6. Douglas, S.M. et al. Self-assembly of DNA into nanoscale three-dimensional shapes. *Nature* **459**, 414–418 (2009).
7. Zhang, D.Y., Seelig, G. Dynamic DNA nanotechnology using strand-displacement reactions. *Nature Chemistry* **3**, 103-113 (2011).
8. Zhang, D.Y., Winfree, E. Control of DNA strand displacement kinetics using toehold exchange. *Journal of the American Chemical Society* **137,** 17303-17314 (2009).
9. Douglas, S.M., Bachelet, I. Church, G.M. A Logic-Gated Nanorobot for Targeted Transport of Molecular Payloads. *Science* **355**, 831-834 (2012).
10. Wang, E. et al. Molecular logic gates on DNA origami nanostructures for microRNA diagnositics. *Analytical Chemistry* **86**, 1932-1936 (2014).

11. Linko, V. and Dietz, H. The enabled state of DNA nanotechnology. *Current Opinion in Biotechnology* **24**, 555-561 (2013).

12. Lund, K. et al Molecular robots guided by prescriptive landscapes. *Nature* **465,** 206-210 (2010).

13. Seelig, G. et al. Enzyme-free nucleic acid logic circuits. *Science* **314**, 1585-1588 (2006).

14. Yin, P. et al. A unidirectional DNA walker that moves autonomously along a track. *Angewandte Chemie International Edition* **43**, 4906-4911 (2004).

15. Douglas, S.M. et al. Rapid prototyping of 3D DNA-origami shapes with caDNAno. *Nucleic Acids Research* **37**, 5001-5006 (2009).

16. Leidl, T. et al. Self-assembly of three-dimensional prestressed tensegrity structures from DNA. *Nature Nanotechnology* **5**, 520-524 (2010).

17. Turowski, D. An investigation of mechanical properties of DNA origami nanostructures. Thesis, Ohio State Universty Knowledge Bank (2012)

Appendix A: Curve Fitting MATLAB Script


```
% written by JMB on 3/15/14 to fit the compiled data from DNA bow
% displacement reaction fluorescence data.

clear all, clc, close all
```

import the excel file

```
% Import the data
[~, ~, raw0_0] = xlsread('C:\Users\Joshua\Desktop\honors thesis\images\image processing\compiling
data_final.xlsx','Sheet1','G7:I12');
[~, ~, raw0_1] = xlsread('C:\Users\Joshua\Desktop\honors thesis\images\image processing\compiling
data_final.xlsx','Sheet1','G17:I22');
raw = [raw0_0,raw0_1];
raw = raw(:,[1,2,3,4,5,6]);

% Create output variable
data = reshape([raw{:}],size(raw));

% Allocate imported array to column variable names
time_bow = data(:,1);
fluor_bow = data(:,2);
std_dev_bow = data(:,3);
time_plas = data(:,4);
fluor_plas = data(:,5);
std_dev_plas = data(:,6);

% Clear temporary variables
clearvars data raw raw0_0 raw0_1 cellVectors;

time_bow = time_bow.*60;
time_plas = time_plas.*60;
% convert the data from minutes to seconds
```

begin fitting process

```
k_plas = [1 fluor_plas(1)]; k_bow = [1 fluor_bow(1)];
% k_plas/k_bow = [initial_value final_value]
%
% The initial value comes from the zero time point without the addition of
% displacement staples, this point was normalized to be one.
%
% The final value is currently taken from the 40 minute trial.
```

```
guess = [50]; % define initial guess --> [time constant]
param_bow_tau = lsqcurvefit(@(param_bow_tau,time_bow)
bow_fit_tau(param_bow_tau,time_bow,k_bow),guess,time_bow,fluor_bow)
% fit the bow fluorescence data to an exponential descending to an
% asymptote SET BY THE DATA and print the value to the screen

param_plas_tau = lsqcurvefit(@(param_plas_tau,time_plas)
bow_fit_tau(param_plas_tau,time_plas,k_plas),guess,time_plas,fluor_plas)
% fit the unstressd control fluorescence data to an exponential descending
% to an asymptote SET BY THE DATA and print the value to the screen

% check the fitted curves (for defined asymptote)

time_check_set = 0:.1:50*60;
fluor_check_bow = bow_fit_tau(param_bow_tau,time_check_set,k_bow);
fluor_check_plas = bow_fit_tau(param_plas_tau,time_check_set,k_plas);

figure
hold on
axis([-1*60 50*60 0 1.1])
plot(time_check_set,fluor_check_bow,'r')
title('DNA bow curve fit to fluorescence data','FontSize',14)
errorbar(time_bow,fluor_bow,std_dev_bow,'b+')
xlabel('time (seconds)','FontSize',14)
ylabel('normalized fluorescence','FontSize',14)
handle = legend('fitted curve','fluorescence data');
set(handle,'FontSize',14);
hold off

figure
hold on
axis([-1*60 50*60 0 1.1])
plot(time_check_set,fluor_check_plas,'r')
title('Unstressed control curve fit to fluorescence data','FontSize',14)
errorbar(time_plas,fluor_plas,std_dev_plas,'b+')
xlabel('time (seconds)','FontSize',14)
ylabel('normalized fluorescence','FontSize',14)
ylabel('normalized fluorescence','FontSize',14)
handle = legend('fitted curve','fluorescence data');
set(handle,'FontSize',14);
hold off

figure
hold on
axis([-1*60 50*60 0 1.1])
plot(time_check_set,fluor_check_bow,'r')
plot(time_check_set,fluor_check_plas,'g')
title('Comparison of fitted curve for the DNA bow and unstressed control','FontSize',14)
xlabel('time (seconds)','FontSize',14)
ylabel('normalized fluorescence','FontSize',14)
handle = legend('DNA bow','unstressed control');
set(handle,'FontSize',14);
hold off
```

```
Local minimum found.

Optimization completed because the size of the gradient is less than
the default value of the function tolerance.



param_bow_tau =

   14.1274


Local minimum found.

Optimization completed because the size of the gradient is less than
the default value of the function tolerance.



param_plas_tau =

  267.2150
```

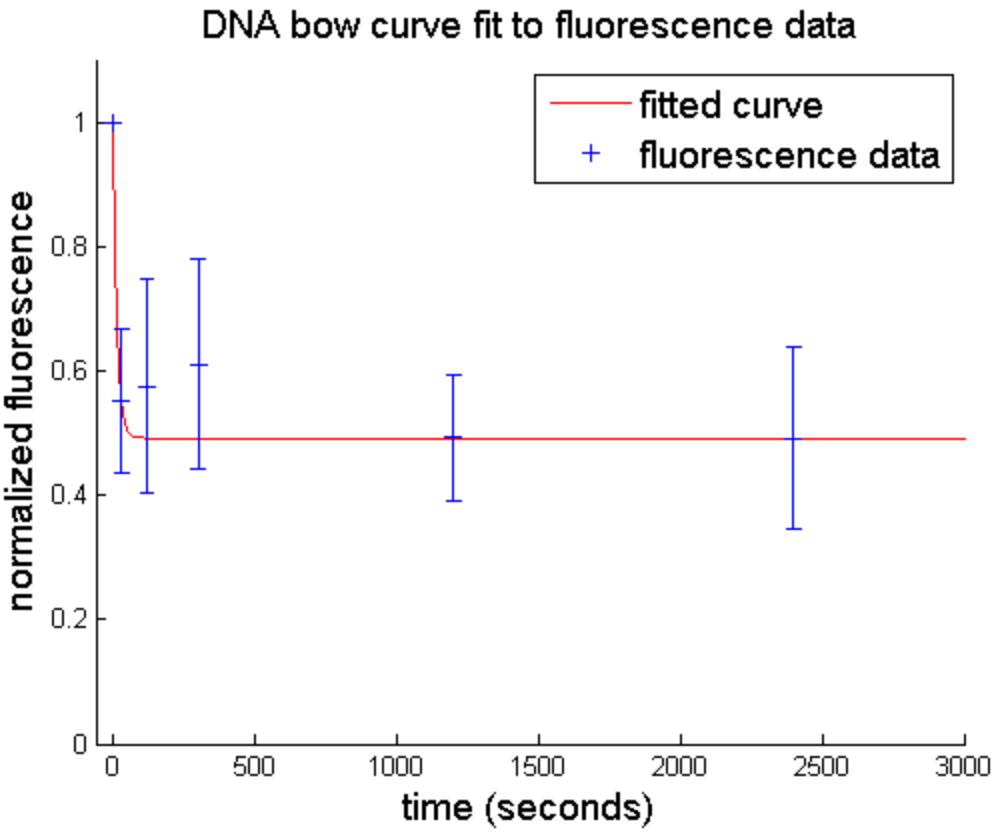

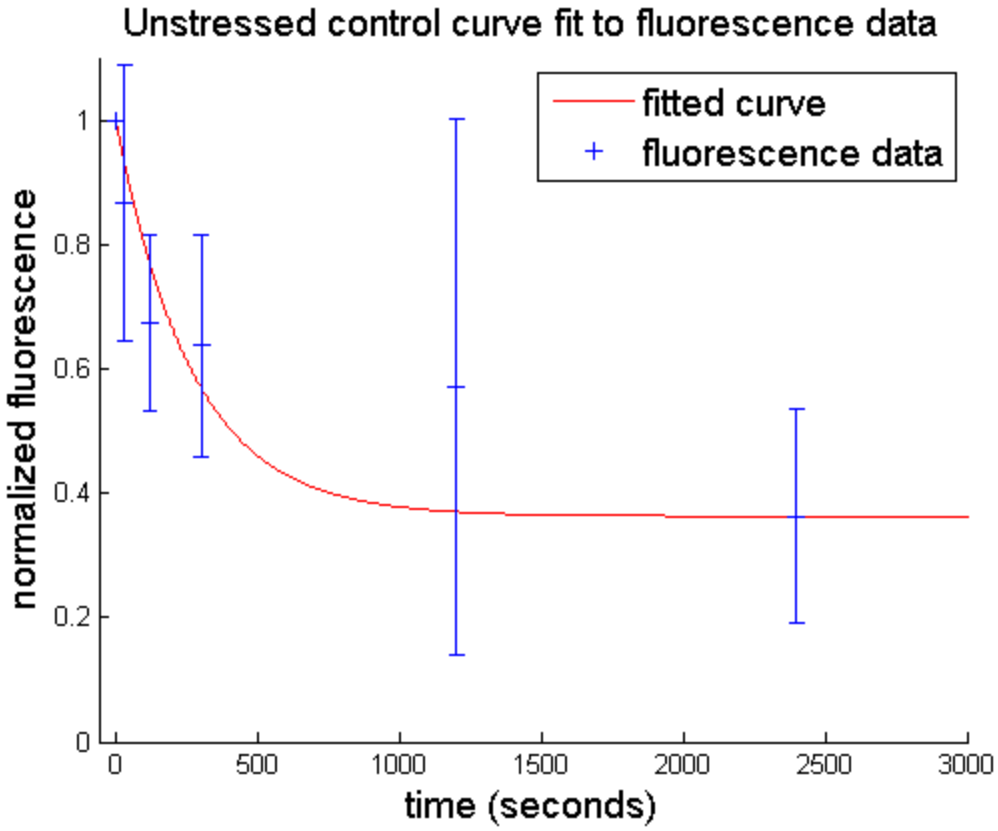

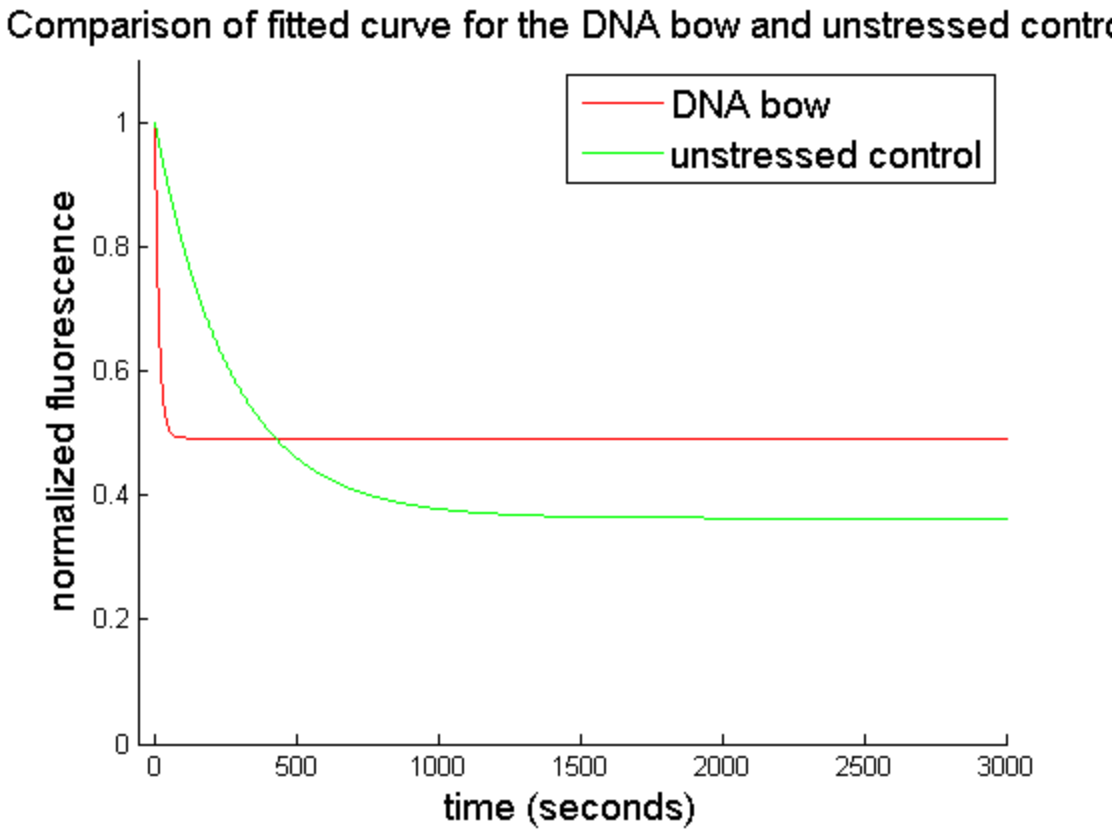

Published with MATLAB® R2012b